

# Critical heat flux in subcooled flow boiling of fluorocarbon liquid on a simulated electronic chip in a vertical rectangular channel

I. MUDAWAR and D. E. MADDOX

Boiling and Two-phase Flow Laboratory, School of Mechanical Engineering, Purdue University, West Lafayette, IN 47907, U.S.A.

(Received 15 April 1988 and in final form 30 June 1988)

**Abstract**—Experiments are performed to correlate and model CHF during subcooled flow boiling of dielectric fluorocarbon (FC-72) liquid on a smooth  $12.7 \times 12.7$  mm<sup>2</sup> simulated electronic chip inside a vertical rectangular channel. Two distinct CHF regimes are established based on flow visualization and experimental data. At low flow velocities, CHF is accompanied by the formation of a continuous vapor blanket and the dryout of a liquid sublayer between the blanket and the chip. Higher velocities reduce the thickness of the vapor blanket and maintain partial contact of subcooled liquid from the core with the chip, leading to the formation of discrete vapor blankets much smaller than the boiling surface of the chip. Experimental data obtained in the lower velocity regime display excellent agreement with predictions of a new CHF model which accounts for the effects of the liquid velocity profile, liquid subcooling and flow geometry.

## 1. INTRODUCTION

THE STUDY of forced convection boiling from an isolated heat source in a channel has become very important in the search for effective methods of cooling high power electronic components. Little fundamental work has been done with this type of flow configuration. However, Katto [1] has shown that, for an internal flow with a short heated length, the boiling process is closer to that of external flow. Previous research with external flow has focused primarily on cross flow over heated cylinders, although some work has been done with other configurations.

In his efforts to develop a generalized correlation for critical heat flux (CHF) in external flow, Katto [2] followed the dimensional analysis of Kutateladze and presented CHF in the form

$$\frac{q_m / \rho_g h_{fg}}{U} = \left[ \frac{\rho_g}{\rho_f}, \frac{\rho_f U^2 d}{\sigma}, \frac{g(\rho_f - \rho_g)d}{\rho_f U^2}, \frac{\mu_g}{\mu_f}, \frac{\rho_f U d}{\mu_f} \right] \quad (1)$$

where  $U$  and  $d$  are the characteristic velocity and length scales associated with the flow boiling system. From studies of flow over a cylinder [3-8] it has been shown that the physical characteristics of CHF at low fluid velocities are similar to those of pool boiling, while at higher velocities the characteristics are much different. Katto suggested that the dimensional analysis of equation (1) could be used to define correlating parameters for both ranges of flow velocity. Neglecting viscosity terms for both cases, and gravity for high flow rates, the following equations were suggested:

low flow rates

$$\frac{q_m}{\rho_g h_{fg}} \left[ \frac{\sigma g(\rho_f - \rho_g)}{\rho_g^2} \right]^{-1/4} = f(\rho_g / \rho_f, d', U') \quad (2)$$

where

$$d' \equiv d[g(\rho_f - \rho_g)/\sigma]^{-1/2} \quad (3)$$

$$U' \equiv U[\sigma g(\rho_f - \rho_g)/\rho_g^2]^{-1/4}; \quad (4)$$

high flow rates

$$\frac{q_m}{G h_{fg}} = f \left[ \frac{\rho_g}{\rho_f}, \frac{G^2 d}{\sigma \rho_f} \right] \quad (5)$$

Two previous studies of CHF for saturated boiling have used configurations very similar to that of the present study. In the first study, Katto and Kurata [9] considered a submerged jet flowing parallel to a small rectangular heater. The fluids tested were water and R-113 with velocity ranging from 1.25 to 10 m s<sup>-1</sup>. CHF data were correlated by the equation

$$\frac{q_m}{G h_{fg}} = 0.186 \left( \frac{\rho_g}{\rho_f} \right)^{0.559} \left( \frac{\sigma \rho_f}{G^2 L} \right)^{0.264} \quad (6)$$

where  $L$  is the length of the heater. The other study was made by Yagov and Puzin [10] for flow of R-12 over a disk heater flush mounted in a rectangular flow channel. Fluid velocities ranged from 0.5 to 12.5 m s<sup>-1</sup> and CHF data were presented by the correlation

$$\frac{q_m}{G h_{fg}} = 0.66 \left( \frac{\rho_g}{\rho_f} \right)^{0.604} \left( \frac{\sigma \rho_f}{G^2 L} \right)^{0.415} \quad (7)$$

One aspect of the present study which has received



from the surface due to vigorous vapor effusion, leaving only a thin liquid sublayer. Their model related the sublayer thickness to the wavelength of the Helmholtz instability by an empirical constant. As in the model of Haramura and Katto [15] for flow boiling, liquid was assumed to enter the sublayer at the mean velocity of the film and CHF was assumed to occur when the total heat supplied to the surface exceeded the latent energy of liquid entering the sublayer. However, Mudawwar *et al.* extended their model to account for liquid subcooling. The ratio of subcooled to saturated CHF was presented in the form

$$\frac{q_{m,\text{sub}}}{q_m} = \left[ 1 + \frac{c_{pf}\Delta T_{\text{sub}}}{h_{fg}} \right]^{1/3} \left[ 1 + 0.16 \frac{\rho_f c_{pf} \Delta T_{\text{sub}}}{\rho_g h_{fg}} \right]^{2/3} \quad (8)$$

where

$$\frac{q_m / \rho_g h_{fg}}{U} = 0.21 \left( \frac{\rho_f}{\rho_g} \right)^{2/3} \left( \frac{\sigma}{\rho_f U^2 L} \right)^{0.42} \quad (9)$$

In the present study, flow boiling experiments were performed with FC-72 (product of 3M Company) on a  $12.7 \times 12.7 \text{ mm}^2$  smooth heater which was flush mounted in the wall of a vertical rectangular channel. This fluid was chosen for its low boiling point ( $T_{\text{sat}} = 56^\circ\text{C}$ ) and unique dielectric properties which make it an ideal candidate for direct immersion cooling of electronic chips. Boiling curves were obtained to determine the parametric influences of velocity and subcooling on CHF. A semi-empirical model is developed to correlate CHF data with respect to both velocity and subcooling. Photographic studies were also conducted both to illustrate the progression of boiling with increasing flux and to aid in the development of the model.

## 2. EXPERIMENTAL APPARATUS

A schematic of the experimental flow loop is shown in Fig. 1. The test section was mounted on a rectangular flow channel which was constructed from an optical grade Lexgard polycarbonate laminate. Figures 2 and 3 show detailed schematics of the flow channel geometry and end reservoirs, respectively. The inlet reservoir contained a nozzle to convert the flow from the annular dimensions of the reservoir to the rectangular area of the flow channel. Immersion heaters in the two reservoirs and a condenser in the outlet reservoir were used to control the system temperature. Vapor trapped in the annular region of the inlet reservoir was routed into the outlet reservoir via a vapor release line. The outlet reservoir drained directly to the magnetically-coupled centrifugal pump, following which a bypass line leading back to the outlet reservoir was used to attain lower velocities in the flow channel. The main flow line contained a water cooled flat plate heat exchanger, used for fluid subcooling, followed by a  $5 \mu\text{m}$  filter and a turbine flowmeter. The filter was mounted in a bypass, which

was closed off during high velocity experiments to reduce flow blockage.

The system was deaerated before each experimental run by circulating fluid through the flow loop and supplying power to the immersion heaters. The mixture of vapor and air was released at the upper section of the outlet reservoir and routed into the pressurization tank. The immersion heater in this tank was then operated to force vapor and air to the secondary condensate tank. Finally a reflux condenser allowed air to escape from the system while recondensing the vapor. At the end of deaeration, the pressurization tank was closed off, and power to its immersion heater was adjusted to attain the desired system pressure. Fluid subcooling was achieved by controlling the flow of cold water to the flat plate heat exchanger. As the fluid in the flow loop cooled and contracted, the channel pressure was maintained by adjusting the power to the pressurization tank.

Two different test heaters were used in this study to simulate high power density electronic chips. The design of the first heater, shown in Fig. 4(a), was based on a calorimeter bar concept. The heat source consisted of an oxygen-free copper bar with a cylindrical cartridge heater embedded in its back end. The heat flux was measured by four thermocouples spaced along the other square-shaped end of the bar. A heater chip attachment was soldered to the heater bar so that different types of surfaces could be tested using a single base heater. A thermocouple embedded in the chip was used to extrapolate the surface temperature based as the measured heat flux. In some experiments three thermocouples were placed along the length of the chip as shown in Fig. 2 in order to measure longitudinal variations in surface temperature. It was found that at the highest flux, the maximum deviation between the upstream and downstream thermocouples was  $2.2^\circ\text{C}$  and the middle thermocouple was generally within 0.5% of the mean value of the extreme temperatures. Thus the middle thermocouple provided a reliable average surface temperature.

Because of the length of the heater bar, the temperature at the back of the heater during high flux experiments was above the limit of the G-10 fiberglass flange. Thus a second heater of shallower construction was built with a higher temperature G-7 fiberglass flange for high flux testing. As shown in Fig. 4(b), the second heat source consisted of a nickel-chromium wire embedded in rectangular grooves machined into one boron nitride plate, and sandwiched with another. The package was then inserted in a square-shaped oxygen-free copper housing which supplied heat to the chip attachment. The housing also provided thermal damping against sudden temperature rise at CHF. A ceramic plate behind the heat source provided insulation against heat loss from the back of the heater. Copper lead wires silver soldered to the nickel-chromium heating element were isolated from the stainless steel back plate by a coating of high temperature

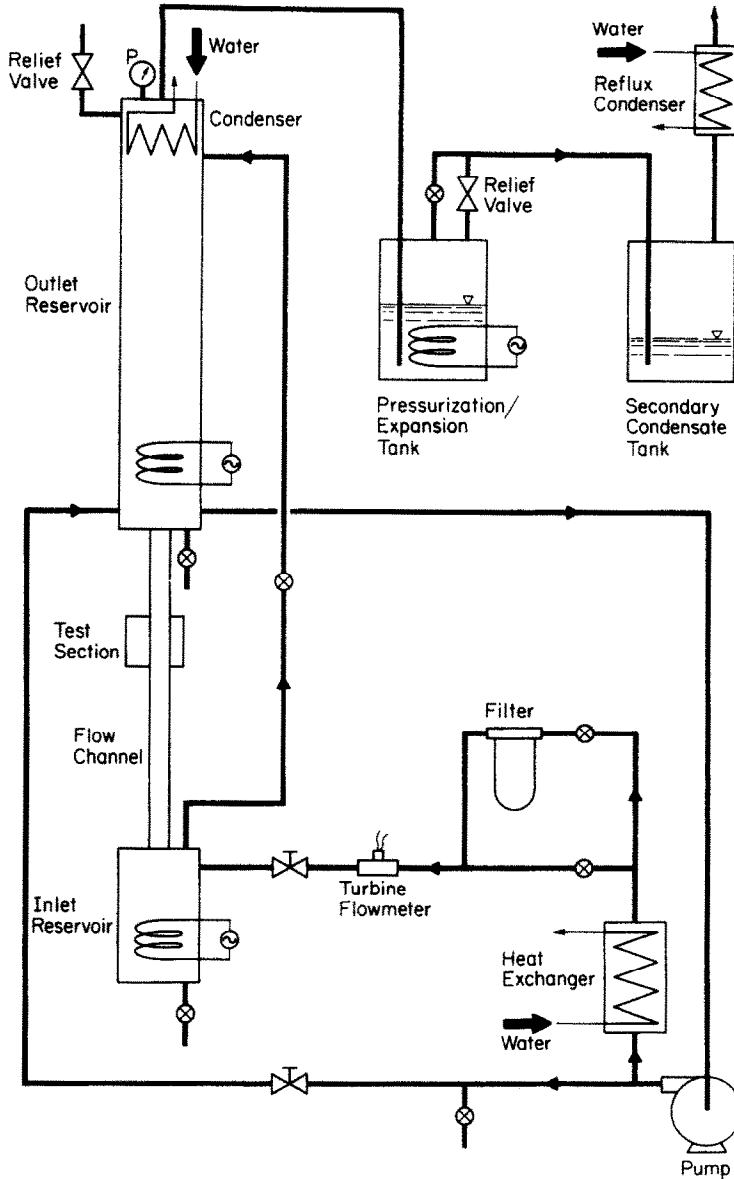


FIG. 1. Schematic diagram of the experimental facility.

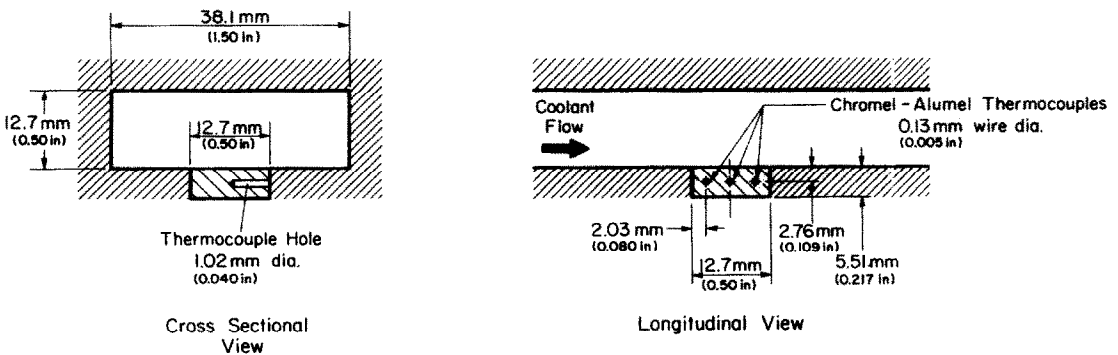


FIG. 2. Schematic of the flow channel cross section and simulated chip.

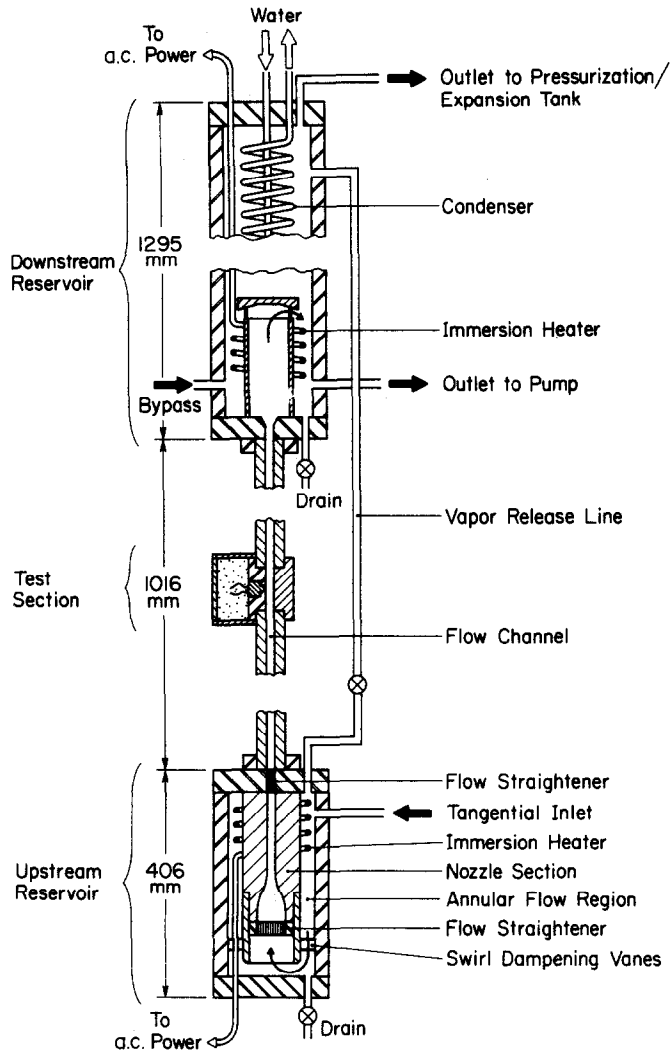


FIG. 3. Cross-sectional diagram of the flow channel and end reservoirs.

epoxy. The heat flux was obtained by measuring electrical power input which was corrected for heat loss. A correction factor was approximated by comparing data for both heaters at  $24^{\circ}\text{C}$  subcooling. The percentage difference was nearly constant at about 4.0% throughout the velocity range. Thus a correction factor of 0.96 was employed with all measurements obtained with the high flux heater.

Data were taken by setting heater power to the desired level and waiting for temperatures in the heater to reach steady-state values. Temperatures and electrical power signals were then measured and recorded using a Keithley System 500 data acquisition system along with a Compaq 286 microcomputer. The uncertainty of all measurement devices in the system was below 0.25% as determined by the makers of these devices.

### 3. RESULTS AND DISCUSSION

Experiments were performed with FC-72 at near atmospheric pressure covering mean flow velocity and

subcooling ranges of  $0.22\text{ m s}^{-1}$  and  $0\text{--}44^{\circ}\text{C}$ , respectively. Properties of saturated FC-72 at atmospheric pressure are given in the Appendix. Some representative experimental runs involved the use of photographic techniques to trace the development of the boiling process prior to, and after CHF. The transparent flow channel provided optical access in a direction normal to the chip surface. Side views of the bubble boundary layer were also photographed to better understand the influence of flow conditions on vapor blanket formation near CHF.

Figure 5 depicts the influence of velocity on boiling at near saturated core conditions. Unfortunately the photographs shown greatly exaggerate the waviness of the substrate surrounding the chip. This was caused by reflections of the powerful light source used in the flow visualization experiments. The recess between the two surfaces was measured by means of a thickness gage before and after each run to ensure flush contact between the chip and the substrate.

As shown in Fig. 5 nucleation always occurred at the downstream edge of the heater, the site of highest

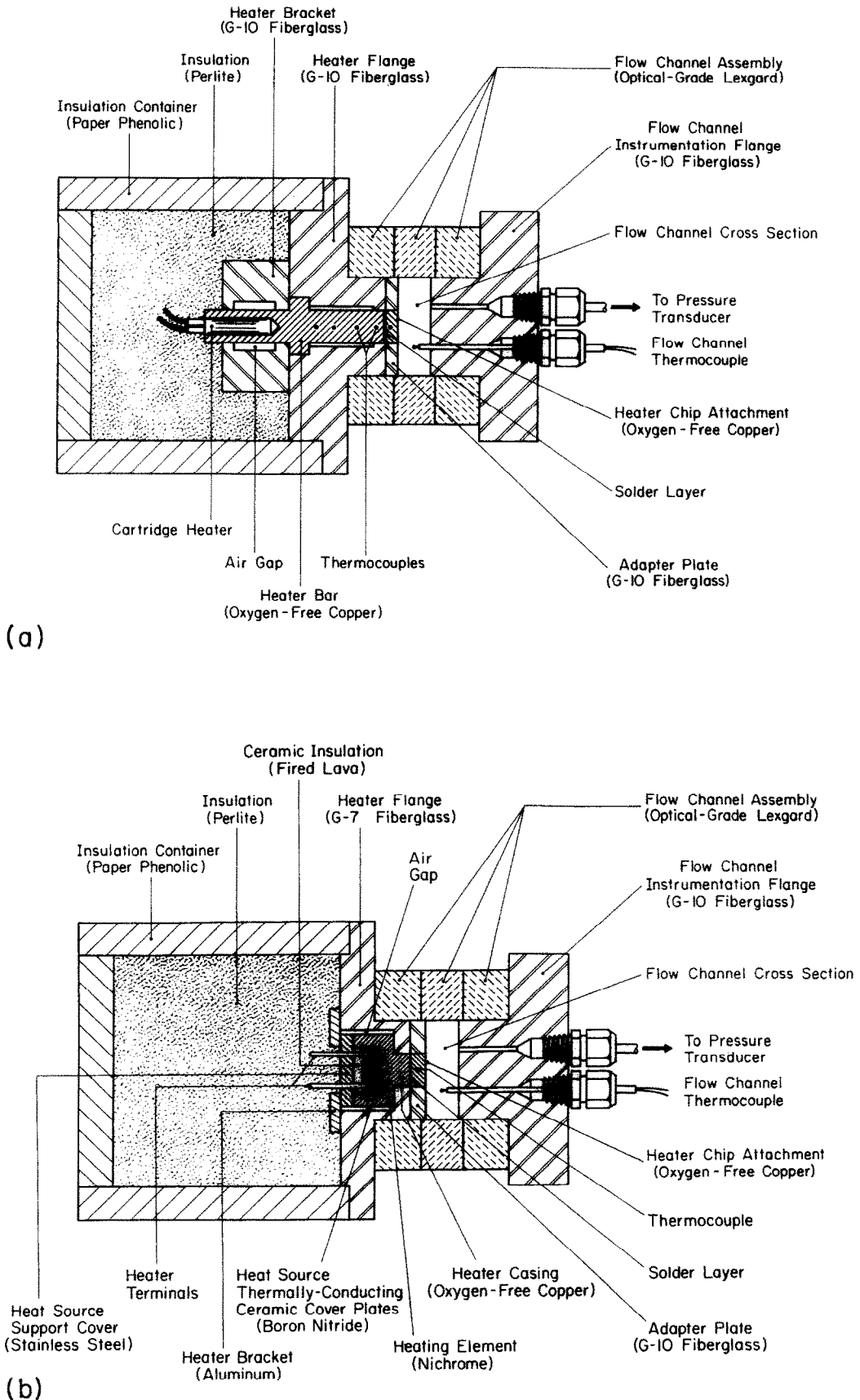


FIG. 4. Construction of test heaters for (a) low flux and (b) high flux measurements.

liquid superheat. Increasing the heat flux resulted in activation of a larger number of cavities and moved the nucleation front toward the upstream edge of the heater. For a velocity of  $0.5 \text{ m s}^{-1}$  boiling incipience was accompanied by rapid nucleation over most of the heated surface. Complete nucleation of the surface occurred at a flux slightly over 30% of CHF. At  $2.25 \text{ m s}^{-1}$  incipience was confined to a small downstream portion of the surface and full nucleation required in excess of 75% of the burnout flux. Bubble size and bubble boundary layer thickness were significantly reduced with increasing velocity. At 99% of CHF a large mass of vapor accumulated over the surface of the chip. At  $U = 0.50 \text{ m s}^{-1}$  the vapor formed a continuous blanket except for nucleation sites at the upstream edge of the heater. The blanket was interrupted by liquid contact with the wall when the velocity was increased to  $2.25 \text{ m s}^{-1}$ , leading to the formation of much smaller blankets which spanned the surface of the chip. Cooling of the surface in both cases was still possible by a liquid sublayer which remained at the wall beneath the vapor layer. Burnout at lower velocities was accompanied by dryout of the sublayer over the downstream portion of the heater while, at high velocities, CHF was triggered by dry patches occurring beneath the small discrete vapor blankets at random locations on the boiling surface. The sublayer dryout phenomenon was most discernible by the naked eye or through the use of high speed video photography since the transient dryout of the sublayer could be clearly detected beneath the vapor blanket.

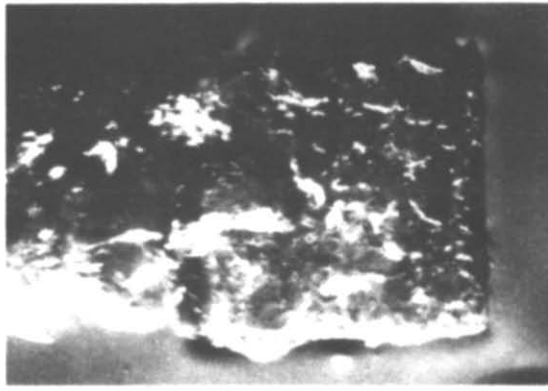
Figure 6 shows successive stages of boiling photographed during a subcooled flow experimental run. The two major effects of subcooling are a reduction of bubble diameter upon departure from the surface and condensation of vapor over a short distance downstream from the heater. However, the CHF mechanism was very similar to that of saturated flow at the same velocity: formation of a continuous vapor blanket and dryout of the liquid sublayer beneath the blanket.

The effect of velocity on the boiling curve is shown in Fig. 7. Figure 7(a) shows data for three flow velocities obtained near saturated conditions. Increasing velocity had a significant enhancement effect in the single-phase and lower nucleate boiling regions, which diminished considerably near CHF. Similar trends were also obtained with similar flow velocities and inlet subcooling of  $15.7^\circ\text{C}$  as shown in Fig. 7(b). Incipience at the lowest velocity was accompanied by a temperature excursion not encountered with higher velocities. There are many factors which influence this excursion, including surface characteristics and the distribution and history of vapor embryos inside wall cavities. In order to achieve consistent surface characteristics for all experimental runs, the surface was treated with a high pressure jet of air, water and abrasive and cleaned with acetone prior to obtaining each

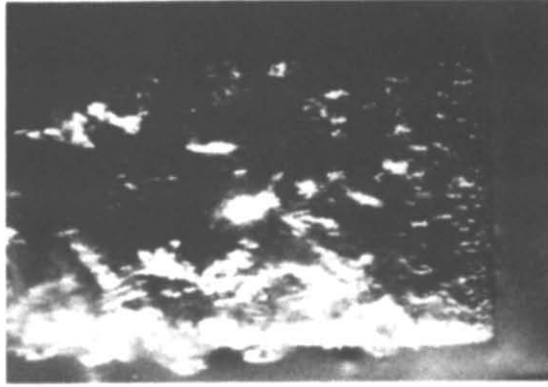
boiling curve. Also the gap between the heater and substrate was carefully sealed with silicone rubber glue to avoid premature incipience from occurring within the gap. The data of Fig. 7(a) were taken without this seal and consequently show no hysteresis. In spite of these precautions, there were inconsistencies in the magnitude of the excursion. Figure 7(b) shows excursions associated with flow velocities of  $0.3$  and  $3.1 \text{ m s}^{-1}$  but none for  $1.0 \text{ m s}^{-1}$ . Nevertheless, it was found that for most boiling experiments increased velocity resulted in a smaller excursion. This trend can be partially explained by the fact that, as the fluid velocity increases, the single-phase heat transfer coefficient also increases, so that the increase in the total heat transfer coefficient at incipience is less pronounced. Another explanation for the large excursion associated with low velocities is the drastic progression of boiling following incipience. Because the maximum surface temperature occurs along the downstream edge of the heater, boiling is most likely to commence in that location. The force created by fluid motion tends to push vapor away from non-boiling portions of the heater. Figure 5 shows that following incipience, lower velocities enable boiling to spread spontaneously over a large portion of the surface, while higher velocities create larger forces on the bubbles, inhibiting rapid propagation of the nucleation front toward the upstream edge of the heater with increased heat flux.

The effect of subcooling on the boiling process is shown in Fig. 8. In this case, enhancement was very substantial near CHF. There was also a general trend of decreased temperature excursion at incipience with increasing subcooling. This trend could also be attributed to the controlled propagation of the nucleation front at incipience. Subcooling results in smaller bubbles, which are less likely to spread to neighboring nucleation sites than the larger bubbles associated with saturated boiling.

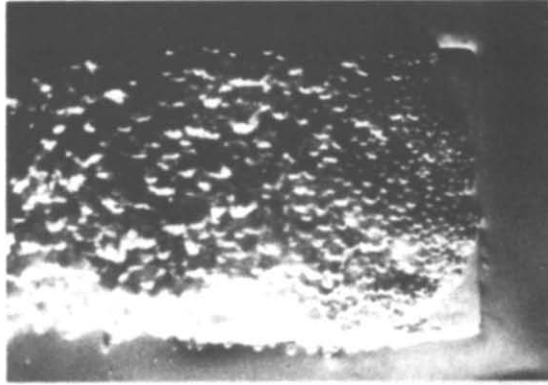
CHF data were taken over a velocity range from  $0.22$  to  $4.1 \text{ m s}^{-1}$  and at levels of subcooling equal to  $4.0$ ,  $14.7$ ,  $24.7$  and  $44.7^\circ\text{C}$ . Figure 9 shows the variation of CHF with velocity at the four subcooling levels. Each of the three cases with higher subcooling shows a transition from a lower slope at lower velocity to a steeper slope at high velocity. This trend is evidence of a marked change in the CHF mechanism associated with increased velocity. From Figs. 5 and 6 it could be concluded that the lower velocity range corresponds to dryout following the formation of a single continuous vapor blanket. On the other hand, CHF in the high velocity range is triggered by dryout beneath blankets which cover smaller portions of the heated surface. Figure 9 shows increased subcooling inducing transition between the two CHF regimes at lower velocity. Apparently the thinning effect subcooling creates on the bubble layer provides greater opportunity for liquid to break through the vapor blanket.



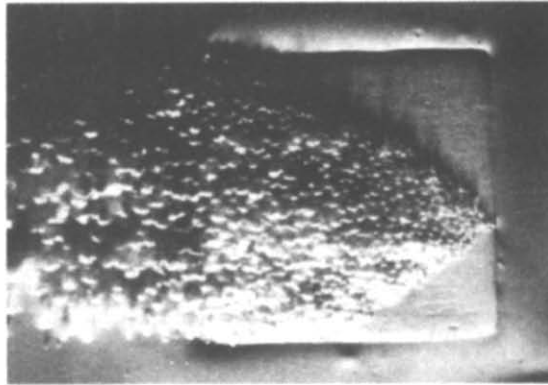
$$q/q_m = 0.99$$



$$q/q_m = 0.77$$



$$q/q_m = 0.30$$



$$q/q_m = 0.17$$



(a)

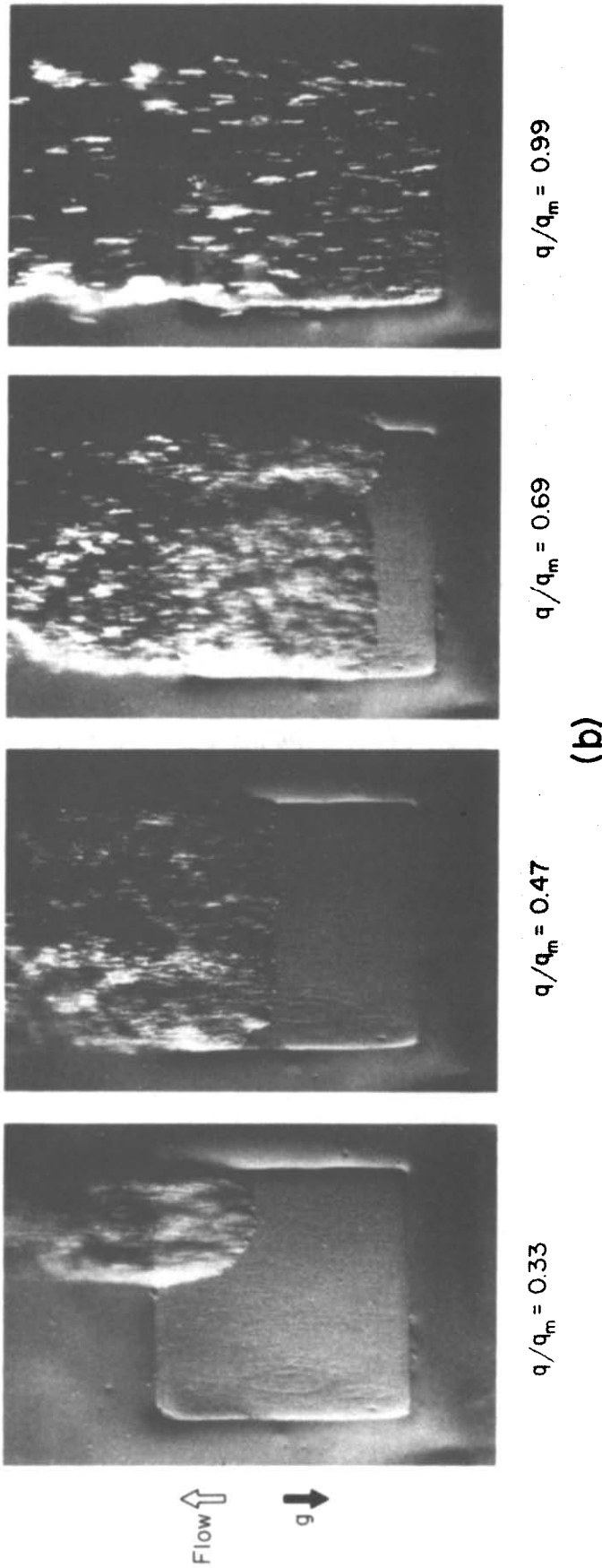


FIG. 5. Successive stages of boiling development for near saturated flow at low and high velocities. (a)  $U = 0.50 \text{ m s}^{-1}$ ,  $\Delta T_{\text{sub}} = 3^\circ\text{C}$ ; (b)  $U = 2.25 \text{ m s}^{-1}$ ,  $\Delta T_{\text{sub}} = 3^\circ\text{C}$ .

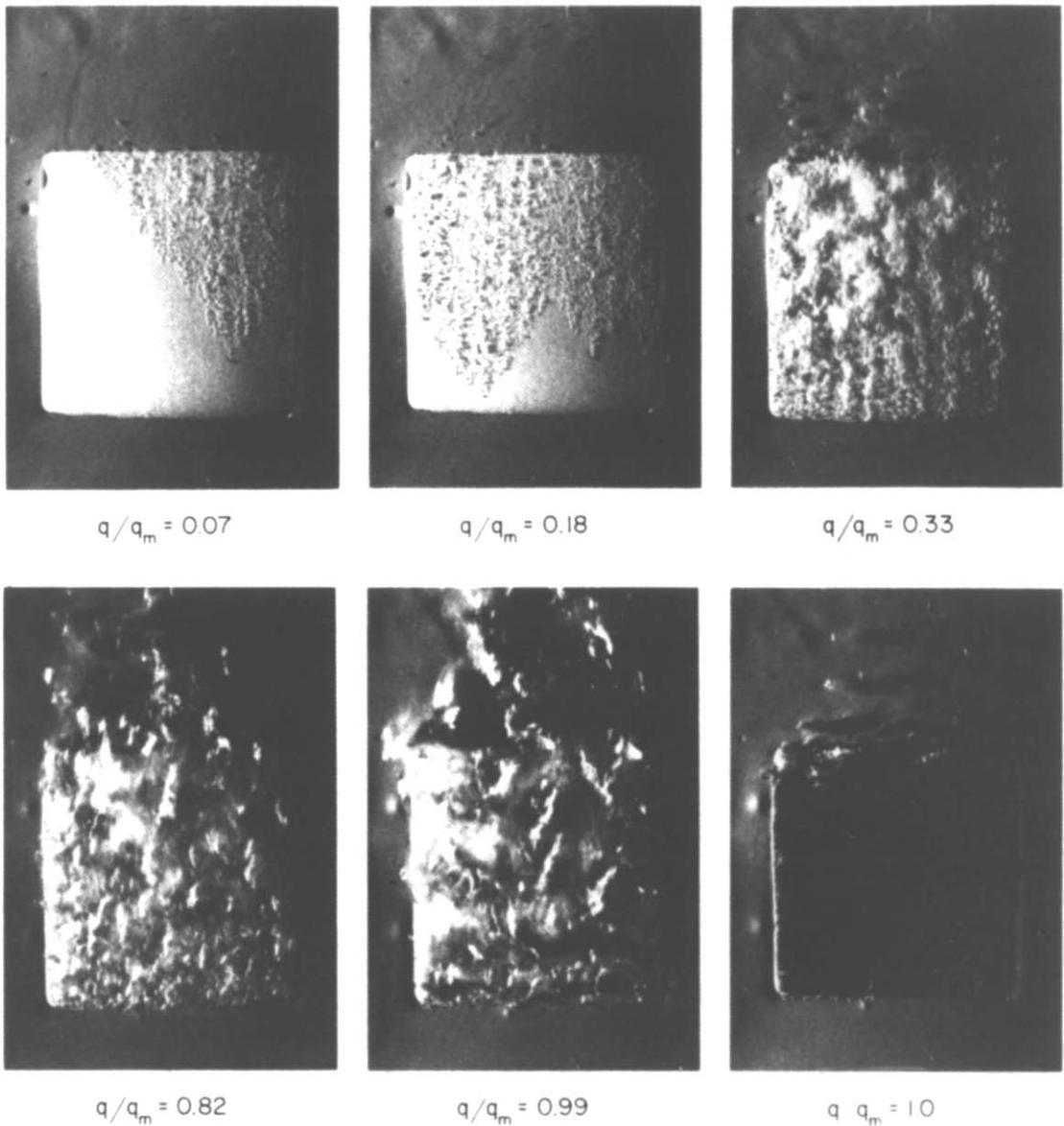


FIG. 6. Successive stages of boiling development in subcooled flow.  $U = 0.50 \text{ m s}^{-1}$ ,  $\Delta T_{\text{sub}} = 15^\circ\text{C}$ .

#### 4. CHF MODEL FOR SUBCOOLED CHANNEL FLOW

Flow visualization and photographic analysis of the development of nucleate boiling prior to, and during CHF reveals the existence of two distinct burnout regimes. As shown in Fig. 9 the low and high velocity CHF regimes are primarily determined by flow velocity and, to some degree, by liquid subcooling.

Figure 10(a) shows a schematic representation of CHF in the low velocity regime. CHF in this regime was characterized by the development of a vapor blanket which thickened in the direction of fluid flow. Just before CHF the blanket became fairly continuous except for the upstream portion of the heater, where severe boiling was still visible. Boiling per-

sisted beneath the upstream portion of the blanket and gradually diminished further downstream. Suppression of nucleate boiling over the downstream portion of the blanket is evidence that evaporation of the liquid sublayer beneath the blanket is the dominant mechanism for heat transfer in that region. Thus, cooling of the heat source just prior to CHF is dependent on boiling and evaporation of liquid entering the sublayer from the subcooled core region of the channel.

Figure 10(b) shows a schematic of high velocity CHF based on flow visualization experiments. This regime differs markedly from the first regime due to a much smaller thickness of the bubble layer compared to low velocity CHF and to the intermittent pattern of vapor blanket formation at CHF. Increasing flow

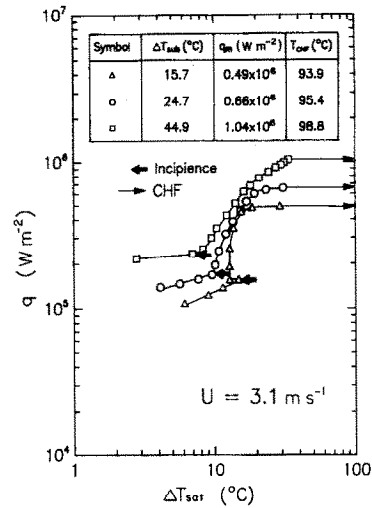
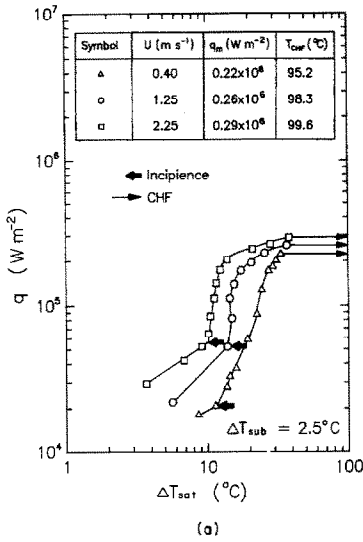


FIG. 8. Effect of subcooling on the boiling curve for  $U = 3.1 \text{ m s}^{-1}$ .

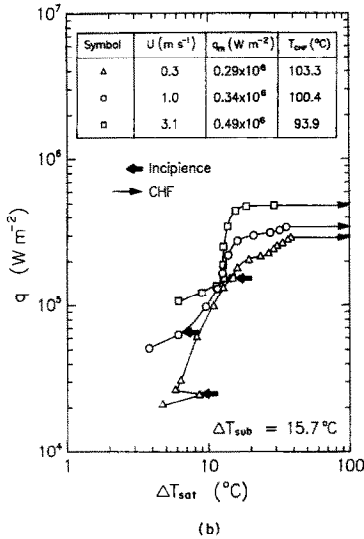


FIG. 7. Effect of flow velocity on the boiling curve for (a)  $\Delta T_{\text{sub}} = 2.5^\circ\text{C}$  and (b)  $\Delta T_{\text{sub}} = 15.7^\circ\text{C}$ .

velocity increased the shear and drag forces on individual bubbles growing at the wall, resulting in rapid departure of bubbles within a very short period following nucleation. Entrained bubbles were also much smaller than those observed in low velocity flow. Just before CHF a thin vapor layer covered the boiling surface as shown in Fig. 5. Unlike low velocity CHF, this layer was composed of continuous blankets much smaller in size than the chip surface. Thus the liquid sublayer was intermittently fed with liquid between these small blankets instead of originating at the upstream edge of the heater. The authors postulate that the breakdown of the vapor layer to smaller blankets at high velocity is the result of a Helmholtz instability occurring at the liquid core-vapor blanket interface *parallel to the wall* due to the large velocity difference between the liquid core and vapor blanket.

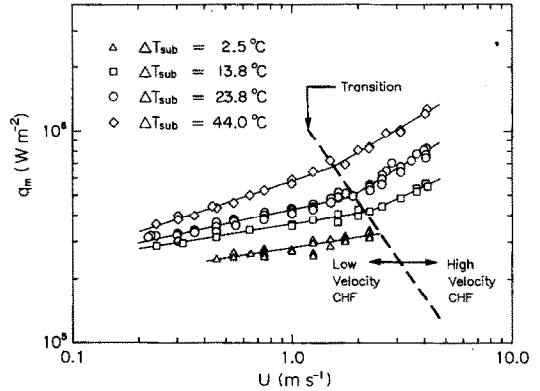


FIG. 9. Variation of CHF with velocity and subcooling.

The proposed model addresses low velocity CHF, which is characterized by the dryout of a liquid sublayer beneath a continuous vapor blanket. This burnout mechanism was proposed by Haramura and Katto [15] for many types of saturated boiling systems. They postulated that, during vigorous boiling, vapor jets leaving the wall are rendered hydrodynamically unstable due to a Helmholtz instability occurring at the interfaces between the jets and the surrounding liquid. This instability quickly develops to form a continuous vapor blanket. Just before CHF the blanket covers the entire boiling surface except for the upstream edge of the heater. They maintained that, following vapor blanket formation, the wall becomes totally dependent on cooling provided by liquid entering the sublayer beneath the blanket. These phenomena are consistent with the observations of Mudawwar *et al.* [16] for CHF in a liquid film of FC-72 flowing at velocities similar to those of the present study.

It should be emphasized that Fig. 10(a) is based on visual studies as well as videographic techniques employed in the present study. Nevertheless, the observed formation and dryout of the thin liquid

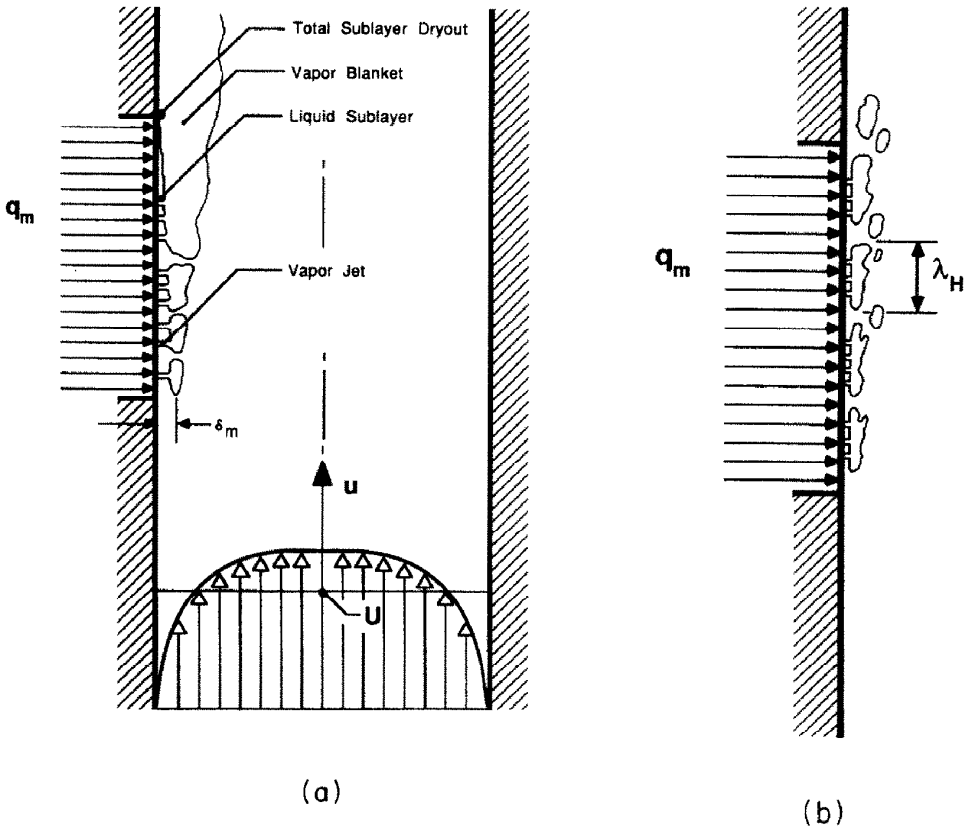


FIG. 10. Schematic representation of (a) low velocity CHF and (b) high velocity CHF.

sublayer beneath a large vapor blanket just before CHF are reminiscent of the CHF observations of Gaertner [14] and Mudawwar *et al.* [16].

The sublayer dryout model of Haramura and Katto was extended by Mudawwar *et al.* to subcooled flow; yet, neither of the two models took into account the external velocity profile effect on the mass flow rate of liquid penetrating into the sublayer.

In the present study a turbulent velocity profile was established in the flow channel upstream of the heater. The laminar sublayer thickness was estimated to be smaller than 0.015 mm for the entire low velocity CHF regime. This thickness was much smaller than the vapor blanket thickness at the upstream edge of the heater which was typically of the order of 0.52 mm. Thus, the fully developed velocity profile upstream of the heater can be approximated as [17]

$$\frac{u}{u^*} = 8.56 \left( \frac{yu^*}{\nu_f} \right)^{1/7} \quad (10)$$

where the friction velocity  $u^*$  is related to the mean velocity  $U$  by

$$u^* = \sqrt{\left( \frac{C_f}{2} \right)} U \quad (11)$$

and the friction coefficient  $C_f$  for turbulent flow

through a smooth channel is given by the Blasius equation

$$C_f = \frac{0.079}{Re^{1/4}} \quad (12)$$

Total dryout of subcooled liquid entering the sublayer at CHF requires that

$$q_m L = \rho_f (c_{pf} \Delta T_{sub} + h_{fg}) \int_0^{\delta_m} u dy \quad (13)$$

where  $\delta_m$  is the liquid sublayer thickness at the upstream edge of the heater. Substituting equations (10)–(12) in dryout criterion (13) gives

$$\frac{q_m / \rho_g h_{fg}}{U} = 1.183 \left( \frac{\rho_f}{\rho_g} \right) \left[ 1 + \frac{c_{pf} \Delta T_{sub}}{h_{fg}} \right] \times \left( \frac{L}{D} \right)^{1/7} \left( \frac{\delta_m}{L} \right)^{8/7} \quad (14)$$

The upstream thickness  $\delta_m$  of the sublayer can be determined from the boiling conditions just before CHF. Mass conservation between vapor jets leaving the surface at velocity  $u_g$ , and the counter flow of liquid approaching the surface at velocity  $u_r$ , requires that

$$\rho_g u_g A_g = \rho_f u_f (A - A_g) \tag{15}$$

where  $A_g$  is the cross-sectional area of a vapor jet and  $A$  the area of one boiling cell which includes a single jet and the surrounding liquid.

Assuming the incoming liquid absorbs the heat transfer from the wall in the form of sensible plus latent energy, the energy balance can be written as

$$q_m A = \rho_g u_g A_g h_{fg} \left[ 1 + C_{sub} \frac{\rho_f c_{pf} \Delta T_{sub}}{\rho_g h_{fg}} \right]. \tag{16}$$

The parameter  $\rho_f c_{pf} \Delta T_{sub} / \rho_g h_{fg}$  is the ratio of sensible heat added to a discrete volume of liquid to the latent heat of an equal volume of vapor released by vapor effusion. The empirical coefficient  $C_{sub}$  accounts for the volumetric ratio associated with bubble-liquid exchange prior to CHF.

Increasing heat flux during vigorous boiling prior to CHF increases the relative velocity between the two phases. The Helmholtz instability occurs when this relative velocity satisfies the criterion [16]

$$|u_g - (-u_f)|^2 \geq \frac{2\pi\sigma(\rho_f + \rho_g)}{\rho_f \rho_g \lambda_{Hm}}. \tag{17}$$

The Helmholtz wavelength  $\lambda_{Hm}$  in equation (17) is proportional to  $\delta_m$ , the length of upstream vapor jets. That is

$$\lambda_{Hm} = C_\lambda \delta_m \tag{18}$$

where  $C_\lambda$  is a constant coefficient of the order of unity. Equation (18) indicates that the liquid subfilm left beneath the large coalescent blanket is formed by breakdown of the vapor jets due to the Helmholtz instability. This breakdown occurs at the first interfacial wave crest near the heated wall when the wave amplitude becomes unstable. Combining equations (15)–(18) gives the following expression for sublayer thickness:

$$\frac{\delta_m}{L} = \psi \left( \frac{\rho_f}{\rho_g} \right) \frac{\left( \frac{\sigma}{\rho_f U^2 L} \right)}{\left( \frac{q_m / \rho_g h_{fg}}{U} \right)^2} \left[ 1 + C_{sub} \frac{\rho_f c_{pf} \Delta T_{sub}}{\rho_g h_{fg}} \right]^2 \tag{19}$$

where

$$\psi \equiv 2\pi C_\lambda \left( 1 + \frac{\rho_g}{\rho_f} \right) \left[ \frac{\frac{A_g}{A}}{1 + \frac{\rho_g}{\rho_f} \frac{A_g}{A}} \right]^2. \tag{20}$$

Following ref. [16], the ratio  $A_g/A$  is assumed to be a very weak function of pressure. Furthermore,  $\rho_g/\rho_f \ll 1$  under normal operating conditions. Thus,  $\psi$  is fairly constant for the conditions of this study.

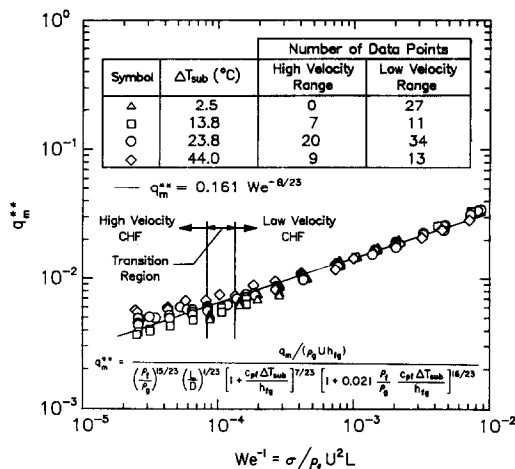


FIG. 11. Comparison of CHF model predictions with experimental data.

Substituting equation (19) for  $\delta_m$  in dryout criterion (14) gives the following expression for CHF:

$$q_m^* = \frac{q_m / \rho_f h_{fg}}{U} = 1.052 \psi^{8/23} \left( \frac{\rho_f}{\rho_g} \right)^{15/23} \left( \frac{\sigma}{\rho_f U^2 L} \right)^{8/23} \times \left( \frac{L}{D} \right)^{1/23} \left[ 1 + \frac{c_{pf} \Delta T_{sub}}{h_{fg}} \right]^{7/23} \times \left[ 1 + C_{sub} \frac{\rho_f c_{pf} \Delta T_{sub}}{\rho_g h_{fg}} \right]^{16/23}. \tag{21}$$

The empirical constants of the CHF model ( $1.052 \psi^{8/23} = 0.161$  and  $C_{sub} = 0.021$ ) were correlated using CHF data corresponding to the low velocity CHF regime only. Figure 11 shows a comparison between model predictions and the entire CHF data base ( $\rho_g/\rho_f = 0.0095-0.0102$ ,  $c_{pf} \Delta T_{sub}/h_{fg} = 0.0170-0.5783$ ). Equation (21) correlates the low velocity data with a mean absolute error of 7.1%. Departure from the correlation is more pronounced in the high velocity CHF regime due to the vapor blanket breakdown phenomenon discussed earlier.

Figure 12 shows a comparison between the present correlation and correlations for saturated CHF in a parallel submerged jet [9] and in a falling liquid film [16]. Also shown are CHF data obtained by Umayá [18] for short heated sections in an annular channel. It is interesting to note the similar slopes of the present correlation and of the falling film study in the low velocity region. The reduced magnitude of CHF in falling films can be attributed to the tendency of free flowing liquid layers to separate away from the surface during severe boiling [16]. The present model shows good agreement with Umayá's data for three different heater lengths. Departure of Umayá's long heater data from the present correlation and from his short heater data may be the result of vapor blanket breakdown over the heated length for  $L/D_H = 9.5$ . The slope of the submerged jet correlation of Katto and Kurata is more characteristic of the high velocity

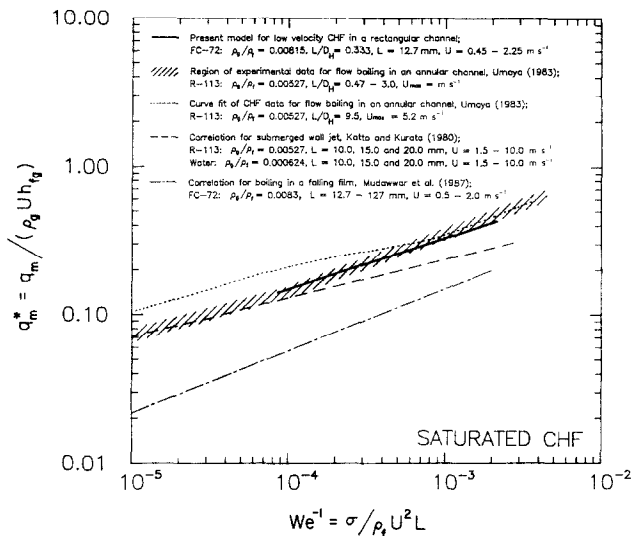


FIG. 12. Comparison of present and previous flow boiling CHF data and correlations.

CHF regime of the present study. Nevertheless the two correlations predict similar values of CHF for  $We^{-1} \sim 1.8 \times 10^{-4}$ .

The CHF dependence on density ratio predicted by equation (21) cannot be verified from the present data since all the experiments were performed near atmospheric pressure, which corresponds to a density ratio of 0.0095–0.0102. In a recent study, Katto *et al.* [8] analyzed data obtained from prior studies for CHF in cross flow of saturated liquid on a uniformly heated cylinder. They presented the following generalized correlation for data over a density ratio range  $\rho_g/\rho_l = 0.005$ –0.4:

$$\frac{q_m}{\rho_g U h_{fg}} = \left[ 0.00588 \frac{\rho_l}{\rho_g} + 0.500 \left( \frac{\rho_l}{\rho_g} \right)^{0.11} \right] \times \left( \frac{\sigma}{\rho_l U^2 d} \right)^{0.42(\rho_g/\rho_l)^{0.0428}} \quad (22)$$

The exponent of the inverse Weber number has a fairly constant value of 0.303–0.404 for the entire density ratio range of equation (22). However, the other density ratio multiplier shows significant departure from the exponential form  $(\rho_l/\rho_g)^n$  commonly employed in CHF correlations. The authors postulate that the variations in the density ratio function of equation (22) are the result of significant changes in the CHF mechanism with pressure. Figure 10 displays one example of the influence of flow velocity alone on CHF. Density ratio (or pressure) also strongly influences the formation and thickness of the vapor blanket and may lead to different sublayer dryout mechanisms. CHF models should then be based on visual and photographic analysis of the boiling surface within well defined ranges of operating conditions. Thus, the usefulness of equation (21) should be limited to low velocity CHF and for density ratios close to those of the present study. It should also be equally

emphasized that the CHF correlation cannot be extrapolated to pool boiling conditions since equation (21) gives  $q_m = 0$  for  $U = 0$ . Again the velocity bound of  $U = 0.22 \text{ m s}^{-1}$  corresponds to the lowest Weber number for which equation (21) is valid.

## 5. SUMMARY

Experiments have been performed to determine the effects of flow velocity and subcooling on CHF from a simulated electronic chip attached to the wall of a vertical rectangular channel. Key results are as follows.

(1) Higher CHF was achieved with higher flow velocities. Increasing velocity reduced the thickness of the bubble layer and enhanced contact of liquid with the heated surface at high fluxes. CHF was also significantly enhanced by increasing the degree of subcooling.

(2) Two distinct CHF regimes were identified through flow visualization and experimental data. Low velocity CHF was accompanied by the formation of a continuous blanket over the entire heated surface and the dryout of a liquid sublayer beneath the blanket. High velocity CHF was characterized by the formation of small vapor blankets occurring randomly over the heated surface due to a Helmholtz instability at the interface between the liquid core and vapor layer in a direction parallel to the surface.

(3) A new model was developed for subcooled low velocity CHF. It was assumed that the vapor blanket associated with this CHF regime is formed by a Helmholtz instability occurring at the interface between vapor jets normal to the surface jets and the surrounding liquid. Burnout was assumed to occur when the sensible and latent energy of the subcooled liquid entering the liquid sublayer beneath the blanket

was smaller than the supplied heater power. The proposed model showed excellent agreement with experimental data.

*Acknowledgement*—Support for this research by the IBM Corporation is gratefully acknowledged.

## REFERENCES

1. Y. Katto, Critical heat flux, *Adv. Heat Transfer* **17**, 1–64 (1985).
2. Y. Katto, Critical heat flux in forced convective flow, *Proc. of the ASME/JSME Thermal Engng Joint Conf.*, Vol. 3, pp. 1–10 (1983).
3. G. C. Vliet and G. Leppert, Critical heat flux for nearly saturated water flowing normal to a cylinder, *J. Heat Transfer* **86**, 59–66 (1964).
4. T. H. Cochran and C. R. Andracchio, Forced convection boiling on cylindrical heaters in water and refrigerant-113, NASA Report D-7553 (1974).
5. J. H. Lienhard and R. Eichhorn, Peak boiling heat flux on cylinders in a cross flow, *Int. J. Heat Mass Transfer* **19**, 1135–1142 (1976).
6. J. H. Lienhard and M. M. Hasan, On predicting boiling burnout with the mechanical energy stability criterion, *J. Heat Transfer* **101**, 276–279 (1979).
7. S. Yilmaz and J. W. Westwater, Effect of velocity on heat transfer in boiling Freon-113, *J. Heat Transfer* **102**, 26–31 (1980).
8. Y. Katto, S. Yokoya, S. Miake and M. Taniguchi, Critical heat flux on a uniformly heated cylinder in a cross flow of saturated liquid over a very wide range of vapor-to-liquid density ratio, *Int. J. Heat Mass Transfer* **30**, 1971–1977 (1987).
9. Y. Katto and C. Kurata, Critical heat flux of saturated convective boiling on uniformly heated plates, *Int. J. Multiphase Flow* **6**, 575–582 (1980).
10. V. V. Yagov and V. A. Puzin, Critical heat fluxes in forced convection boiling of refrigerant-12 under conditions of local heat sources, *Heat Transfer—Sov. Res.* **16**, 47–55 (1984).
11. S. S. Kutateladze, *Fundamentals of Heat Transfer* (Edited by R. D. Cess), p. 387. Academic Press, New York (1963).
12. G. C. Vliet and G. Leppert, Critical heat flux for subcooled water flowing normal to a cylinder, *J. Heat Transfer* **86**, 68–74 (1964).
13. G. Meyer, E. S. Gaddis and A. Vogelpohl, Critical heat flux on a cylinder of large diameter in a cross flow, *Proc. 8th Int. Heat Transfer Conf.*, Vol. 5, pp. 2125–2130 (1986).
14. R. F. Gaertner, Photographic study of nucleate pool boiling on a horizontal surface, *J. Heat Transfer* **87**, 17–29 (1965).
15. Y. Haramura and Y. Katto, A new hydrodynamic model of critical heat flux applicable widely to both pool and forced convection boiling on submerged bodies in saturated liquids, *Int. J. Heat Mass Transfer* **26**, 389–399 (1983).
16. I. A. Mudawwar, T. A. Incropera and F. P. Incropera, Boiling heat transfer and critical heat flux in liquid films falling on vertically-mounted heat sources, *Int. J. Heat Mass Transfer* **30**, 2083–2095 (1987).
17. J. M. Kay and R. M. Nedderman, *Fluid Mechanics and Transfer Processes*, p. 171. Cambridge University Press, Cambridge (1985).
18. M. Umayama, Critical heat flux for annular channels with small heated length to heated equivalent diameter ratios, M.Sc. Thesis, Dept. of Mech. Engng, University of Tokyo (1983).

## APPENDIX. PROPERTIES OF FC-72

FC-72 is an inert dielectric fluid produced by 3M Company for direct immersion cooling of electronic chips. It is derived from hydrocarbon compounds by replacing all the carbon-bound hydrogen atoms with fluorine atoms. Most of the property values used in this study are based on tables supplied from the Industrial Chemical Products Division of 3M Company. The surface tension was measured at the Boiling and Two-phase Flow Laboratory of Purdue University using a Kruss K8 ring-type interfacial tensiometer equipped with a constant temperature bath. The properties of saturated FC-72 at atmospheric pressure are listed in Table A1.

Table A1. Properties of saturated FC-72 at atmospheric pressure

$T_{\text{sat}}$ (°C)	$c_{pf}$ (J kg <sup>-1</sup> K <sup>-1</sup> )	$h_{fg}$ (J kg <sup>-1</sup> )	$\rho_f$ (kg m <sup>-3</sup> )	$\rho_g$ (kg m <sup>-3</sup> )	$\sigma$ (N m <sup>-1</sup> )
56	1096	84 730	1620	13.01	0.00948

## FILM THERMIQUE CRITIQUE DANS L'ÉCOULEMENT, AVEC ÉBULLITION SOUS-REFROIDIE, DE FLUOROCARBURE LIQUIDE SUR UNE CHIP ÉLECTRONIQUE DANS UN CANAL RECTANGULAIRE VERTICAL

**Résumé**—Des expériences sont faites sur le CHF pendant l'écoulement, avec ébullition sous-refroidie, d'un fluorocarbure diélectrique (FC-72) liquide sur une simulation de chip électronique lisse 12,7 × 12,7 mm<sup>2</sup>, dans un canal rectangulaire et vertical. Aux faibles vitesses d'écoulement, le CHF est accompagné de la formation d'une nappe continue de vapeur et de l'assèchement d'une sous-couche liquide entre la nappe et la chip. De grandes vitesses réduisent l'épaisseur de la nappe de vapeur et maintiennent un contact partiel de liquide sous-refroidi du coeur de l'écoulement avec la chip. Des données expérimentales obtenues dans le régime de basse vitesse sont en bon accord avec les prédictions d'un nouveau modèle de CHF qui tient compte des effets du profils de vitesse du liquide, du sous-refroidissement du liquide et de la géométrie d'écoulement.

**DIE KRITISCHE WÄRMESTROMDICHTEN AN EINEM SIMULIERTEN  
ELEKTRONISCHEN CHIP BEI UNTERKÜHLTEN STRÖMUNGSSIEDEN EINES  
FLUORKOHLENSTOFFS IN EINEM VERTIKALEN RECHTECKKANAL**

**Zusammenfassung**—Es wurden Versuche durchgeführt zur Korrelation und Modellierung der kritischen Wärmestromdichte (CHF) an einem simulierten, ebenen,  $12,7 \times 12,7$  mm<sup>2</sup> großen, elektronischen Chip bei unterkühltem Strömungssieden von dielektrischem Fluorkohlenstoff (FC-72) in einem vertikalen Rechteckkanal. Zwei ausgeprägte CHF-Bereiche wurden anhand der experimentellen Daten und der Strömungsbeobachtungen festgestellt. Bei niedrigen Strömungsgeschwindigkeiten bildet sich bei der CHF ein geschlossener Dampffilm, und die Flüssigkeitsunterschicht zwischen dem Dampffilm und dem Chip trocknet aus. Höhere Strömungsgeschwindigkeiten verringern die Dampffilmdicke und führen zu stellenweisem Kontakt der unterkühlten Flüssigkeit aus dem Kern mit dem Chip. Dies hat die Bildung von einzelnen Dampfzonen zur Folge, die viel kleiner als die Siedeoberfläche des Chips sind. Die im Bereich niedriger Geschwindigkeiten aufgenommenen Versuchsdaten stimmen sehr gut mit den Werten eines neuen CHF-Modells überein, das den Einfluß des Geschwindigkeitsprofils der Flüssigkeit, der Flüssigkeitsunterkühlung und der Strömungsgeometrie berücksichtigt.

**КРИТИЧЕСКИЙ ТЕПЛОВОЙ ПОТОК ПРИ КИПЕНИИ ЖИДКОГО НЕДОГРЕТОГО  
ФТОРОУГЛЕРОДА, ОБТЕКАЮЩЕГО МОДЕЛЬНЫЙ ЭЛЕКТРОННЫЙ ЧИП В  
ВЕРТИКАЛЬНОМ ПРЯМОУГОЛЬНОМ КАНАЛЕ**

**Аннотация**—Проведены эксперименты обобщения и моделирования критического теплового потока (КТП) при кипении жидкого недогретого диэлектрического фтороуглерода (ФУ-72), обтекающего модельный электронный чип в вертикальном прямоугольном канале. На основе визуализации потока и экспериментальных данных установлены два отчетливо выраженных режима КТП. При низких скоростях течения КТП связан с образованием сплошного слоя пара и высыханием жидкого подслоя между паровым слоем и поверхностью. При более высоких скоростях толщина парового слоя уменьшается и происходит частичное контактирование между недогретой жидкостью и поверхностью, что приводит к образованию дискретных паровых слоев, размер которых намного меньше поверхности кипения. Экспериментальные данные, полученные в режиме небольших скоростей, хорошо согласуются с расчетами по новой модели КТП, в которой учитываются эффекты профиля скорости жидкости, ее недогрева и геометрии течения.